Supplementary information for: "Critical role of water on the synthesis and gelling of γ-In_2S_3 nanoribbons with giant aspect ratio."

Lilian Guillemeney[1], Laurent Lermusiaux[1], Patrick Davidson[2], Austin Hubley[1,3], Stefano Pierini[4], Debora Pierucci[5], Gilles Patriarche[5], Bruno Canut[6], Emmanuel Lhuillier[4], Benoît Mahler[3], and Benjamin Abécassis[*1]

[1]ENSL, CNRS, Laboratoire de Chimie UMR 5182, 46 allée d'Italie, 69364 Lyon France
[2]Laboratoire de Physique des Solides, Université Paris-Saclay, CNRS, 91405 Orsay
[3]Univ Lyon, Université Claude Bernard Lyon 1, CNRS, Institut Lumiere Matiére (iLM), F-69622 Villeurbanne, France
[4]Sorbonne Université, CNRS, Institut des NanoSciences de Paris, INSP, F-75005 Paris, France
[5]Centre de Nanosciences et de Nanotechnologies, CNRS, Université Paris Saclay, 91120 Palaiseau, France
[6]Ecole Centrale de Lyon, CNRS, INSA Lyon, Université Claude Bernard Lyon 1, CPE Lyon, CNRS, INL, UMR5270, Ecully 69130, France

1 Uncertainty calculations

The global uncertainty given for each spatial dimension with a 95% confidence interval is $U = 2.\sqrt{U_A^2 + U_B^2}$ with $U_A = \frac{\sigma}{\sqrt{n}}$ the A-type uncertainty (σ is the square deviation of the statistical series and n the number of measurements, generally more than one hundred to be statistically relevant). B-type uncertainties are given by U_B which is evaluated by repeating the same measurement 50 times.
For a quantity X (e.g. the ones in the next paragraph), product of two other quantities Y and Z, the uncertainty on X, ΔX, is given by: $\Delta X = X \times \sqrt{\left(\frac{\Delta Y}{Y}\right)^2 + \left(\frac{\Delta Z}{Z}\right)^2}$ where ΔY and ΔZ are the uncertainties on the quantities Y and Z.

2 Oleylamine surface density from XPS measurements

Assuming that the volume of one ribbon is $(7.2 \pm 0.5) \times 10^6$ Å^3 (from statistical measurements done previously by TEM) and that the volume of one unit-cell of γ-In_2S_3 is 118.5 Å^3, we deduce that one NR is made of $(6.1 \pm 0.4) \times 10^4$ cells. Each crystallographic cell contains 4 indium atoms, leading to $(2.4 \pm 0.2) \times 10^5$ indium atoms per NR. As the atomic ratio between indium and nitrogen is (4.4±0.6) (considering an XPS error on Indium and Nitrogen percentages of 10%), we get the number of oleylamine molecules bonded to the NR surface (i.e. $(5.6 \pm 0.9) \times 10^4$ molecules). The surface accessible for oleylamine molecules is $(2.02 \pm 0.08) \times 10^4$ nm^2 (top plus bottom nanoribbon faces), so that the oleylamine ligand density is 2.3 ± 0.8 molecules.nm^{-2} (confidence interval of 95%). This ligand density is of the same order of magnitude as other surface ligand densities already reported in the literature for nanomaterials, which ranges from 0.5 to 5.5 ligands.nm^{-2}[1–4]. For instance, *Anderson et al.* determined by NMR a ligand density of 4.3 oleate.nm^{-2} for PbS QD and 3.3 oleate.nm^{-2} for CdSe QD[2]. *Fritzinger et al.* reported a value for CdSe QD of (4.6 ± 0.4) oleate.nm^{-2}[5].

3 Temperature dependence

All synthesis parameters (reaction time and volume, stoichiometry of precursors, amount of water, and ramp of temperature) are kept constant; we only vary the reaction temperature. These experiments were made with a Linkam heating stage with samples filled into glass capillaries. We checked that this setup does not affect the reaction which remains identical to the solvothermal process. 15 μL of the reaction mixture are poured into a glass capillary of 1 mm diameter which is then flame-sealed. At the end of each reaction, the capillary is broken to purify the reaction medium by dispersion in a mixture of toluene and ethanol and centrifugation. The precipitate is then redispersed in THF and drop-casted onto a carbon-coated copper grid for TEM observations. This setup allows for precise control of experimental temperature parameters such as the ramp of temperature

(thanks to a nitrogen gas flow) and the final temperature, and for minimum temperature overshoot. Additionally, the use of capillaries ensures that all samples react in exactly the same conditions: homogeneous heating, reaction volume, no contact with air. Optimal control and tuning of each reaction parameter can then be achieved, which allows for meaningful comparison of the different outcomes of the reaction.

We found that temperature can be used to control the aspect ratio and length of the nanoribbons. For a reaction time reduced to 15 minutes, no objects are synthesized at 180°C. However, when the reaction temperature is increased, NR become more numerous, longer, and wider, reaching up to 4 micrometers in length when the synthesis is performed at 250°C (Figure S9, Table S0). As expected, increasing the temperature speeds up the reaction kinetics and favors longer and wider ultrathin NR. The same trend is observed when the reaction time is increased at a given temperature (230°C). Indeed, after 15 minutes of reaction, NR are (238 $\pm$ 20) nm long and (6.0 $\pm$ 0.3) nm wide. After 2 hours of reaction, NR are (1.1 $\pm$ 0.2) μm long and (6.3 $\pm$ 0.3) nm wide. Increasing the reaction time by a factor of 8 leads to five times longer NR with the same width. This highlights the highly anisotropic character of the NR growth along their main axis.

Reaction Temperature	180°C	200°C	230°C	250°C
Averaged length	No NR	(97 $\pm$ 6) nm	(238 $\pm$ 20) nm	(1.6 $\pm$ 0.1) μm
Averaged width	No NR	(5.2 $\pm$ 0.2) nm	(6.0 $\pm$ 0.3) nm	(9.4$\pm$ 0.3) nm

Table S0. Average measured dimensions of In_2S_3 as a function of the reaction temperature.

References

1. Hens, Z. & Martins, J. C. A Solution NMR Toolbox for Characterizing the Surface Chemistry of Colloidal Nanocrystals. *Chem. Mater.* **25**, 1211–1221, DOI: 10.1021/cm303361s (2013).
2. Anderson, N. C., Hendricks, M. P., Choi, J. J. & Owen, J. S. Ligand Exchange and the Stoichiometry of Metal Chalcogenide Nanocrystals: Spectroscopic Observation of Facile Metal-Carboxylate Displacement and Binding. *J. Am. Chem. Soc.* **135**, 18536–18548, DOI: 10.1021/ja4086758 (2013).
3. Antanovich, A. *et al.* A strain-induced exciton transition energy shift in CdSe nanoplatelets: The impact of an organic ligand shell. *Nanoscale* **9**, 18042–18053, DOI: 10.1039/C7NR05065H (2017).
4. Widmer-Cooper, A. & Geissler, P. L. Ligand-Mediated Interactions between Nanoscale Surfaces Depend Sensitively and Nonlinearly on Temperature, Facet Dimensions, and Ligand Coverage. *ACS Nano* **10**, 1877–1887, DOI: 10.1021/acsnano.5b05569 (2016).
5. Fritzinger, B., Capek, R. K., Lambert, K., Martins, J. C. & Hens, Z. Utilizing Self-Exchange To Address the Binding of Carboxylic Acid Ligands to CdSe Quantum Dots. *J. Am. Chem. Soc.* **132**, 10195–10201, DOI: 10.1021/ja104351q (2010).

4 Supplementary figures

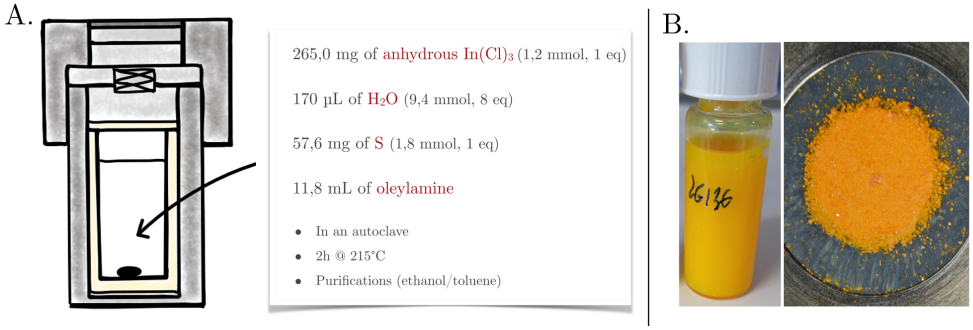

Figure S1. (a) Scheme of the experimental conditions. (b) Left: colloidal solution of nanoribbons dispersed in toluene. Right: nanoribbons in powder form.

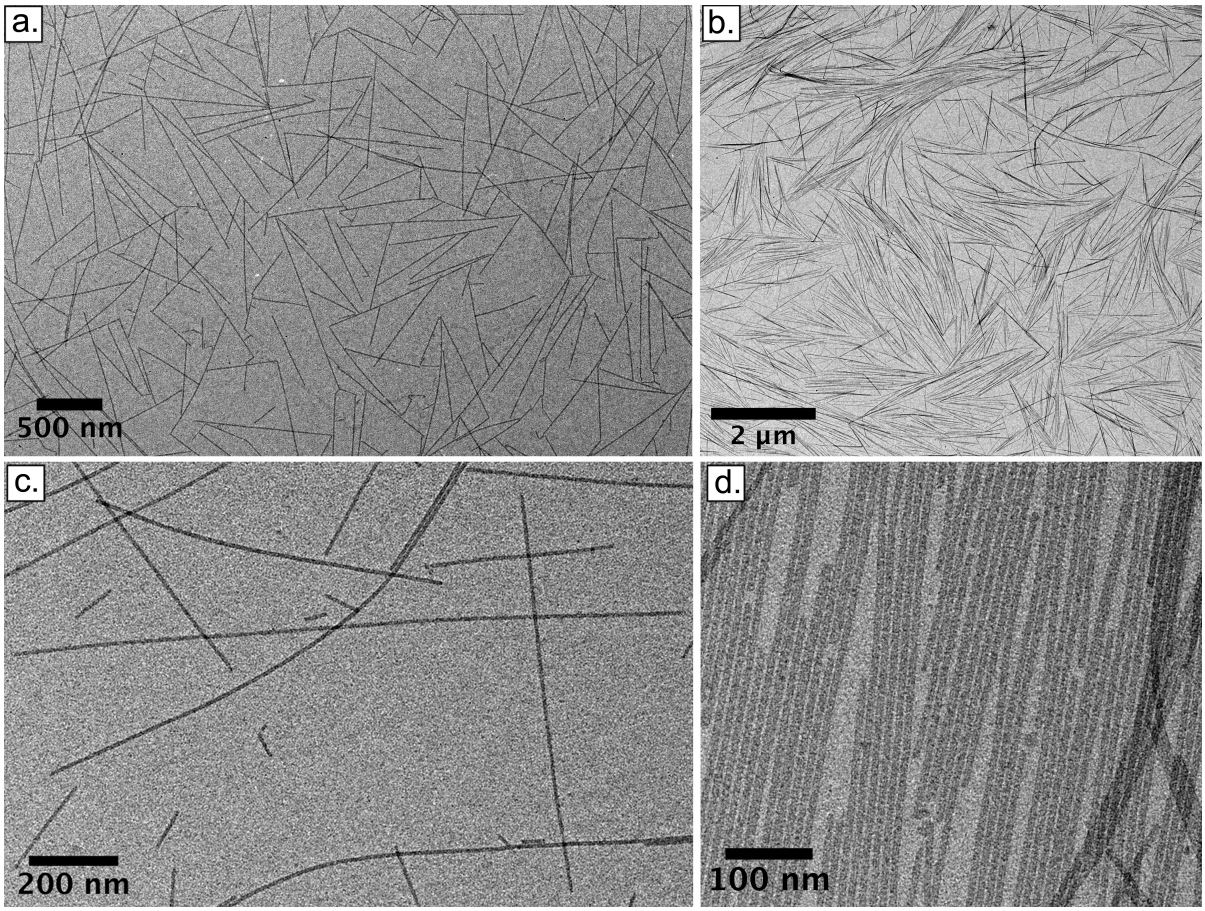

Figure S2. TEM images at different magnifications of In_2S_3 NR lying flat.

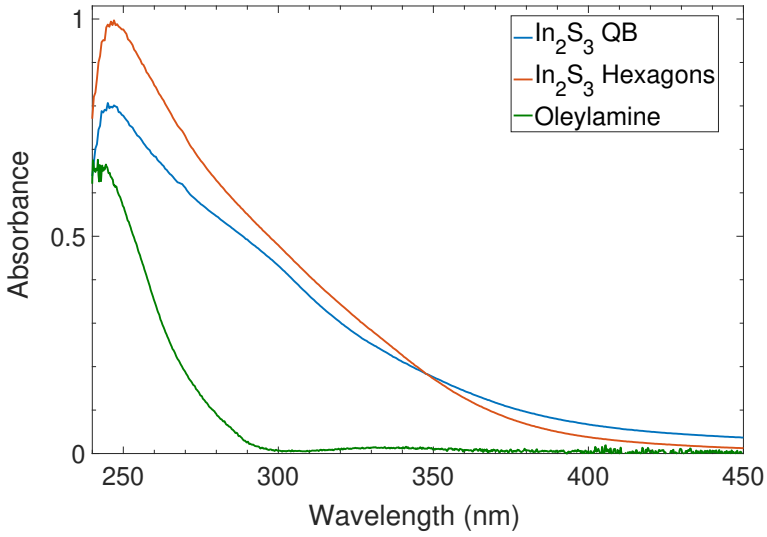

Figure S3. UV-visible absorption spectra of In_2S_3 hexagons (red) and NR (blue) in THF at a concentration around 0.027 $g.L^{-1}$. These spectra have similar shapes, with maximum absorption at 247 nm and broad absorption tail extending up to approximately 550 nm, so that both solutions are yellow. In green is the UV-vis spectrum of oleylamine in THF at 0.03 $mol.L^{-1}$, showing the contribution of oleylamine as surface ligand in the absorption of In_2S_3 nanomaterials.

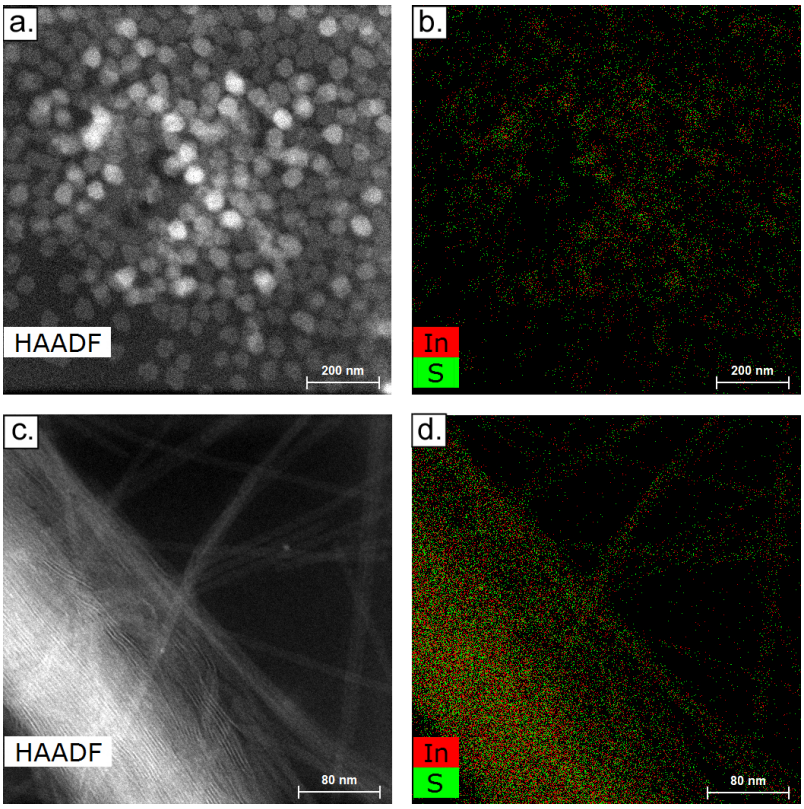

Figure S4. Elemental mapping of In_2S_3 hexagons and NR by Energy Dispersive X-Ray Spectroscopy (EDX). (a, c) HAADF-STEM images of In_2S_3 hexagons and NR. (b, d) Indium and sulfur elemental mapping of these sample areas.

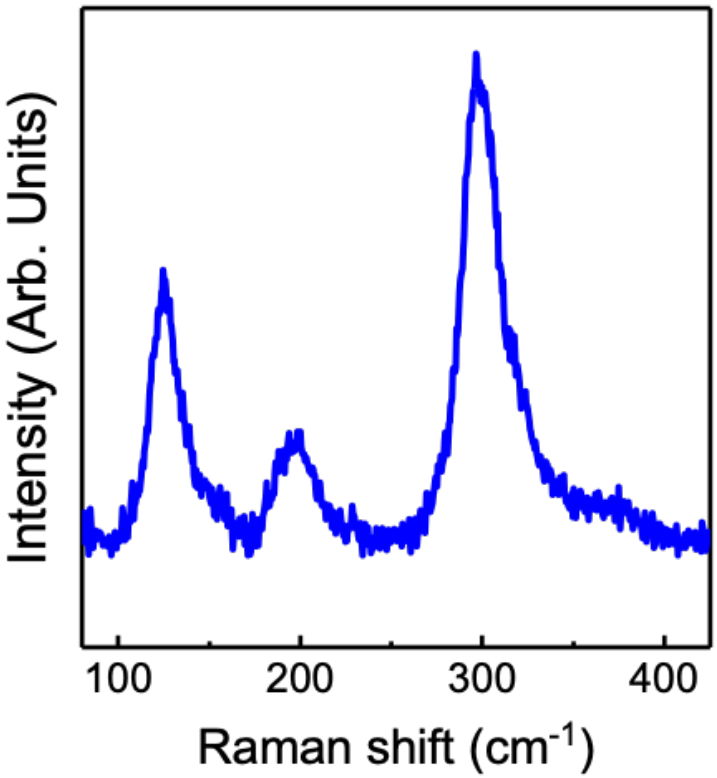

Figure S5. Raman spectrum of In_2S_3 nanoribbons. γ-In2S3 belongs to the D^3_{3d} point group symmetry which presents, as mentioned in the main text, 9 Raman active modes. These modes are given by the combination of $3A_{1g} + 3E_g$. A univocal identification of each vibrational mode requires a DFT calculation of the phonon dispersion curve.

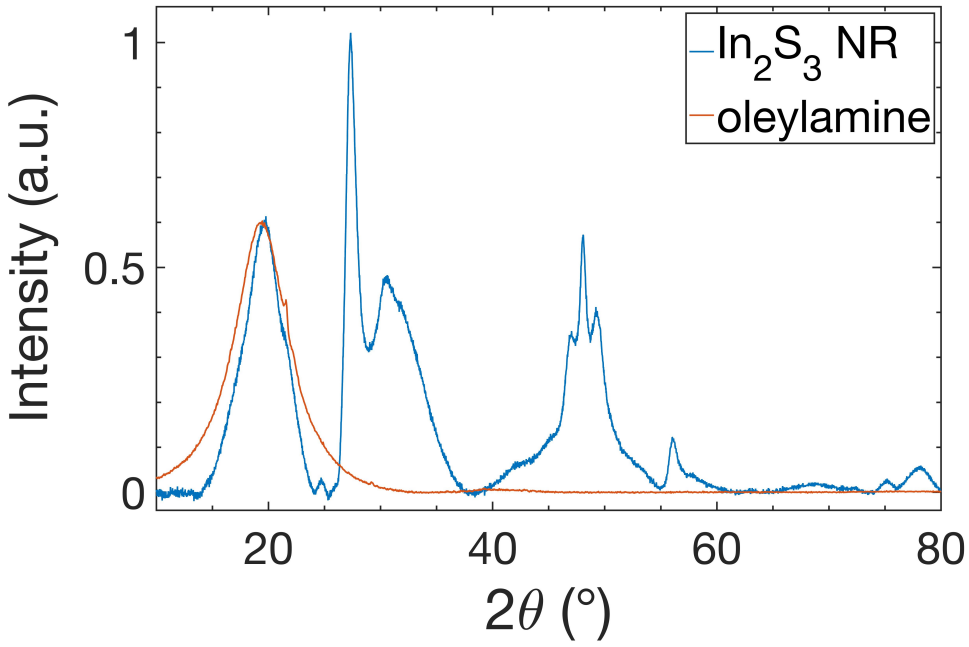

Figure S6. X-ray diffractograms of In_2S_3 NR (blue) and pure oleylamine (red). Note the presence of a diffraction peak at 19.5° for both products.

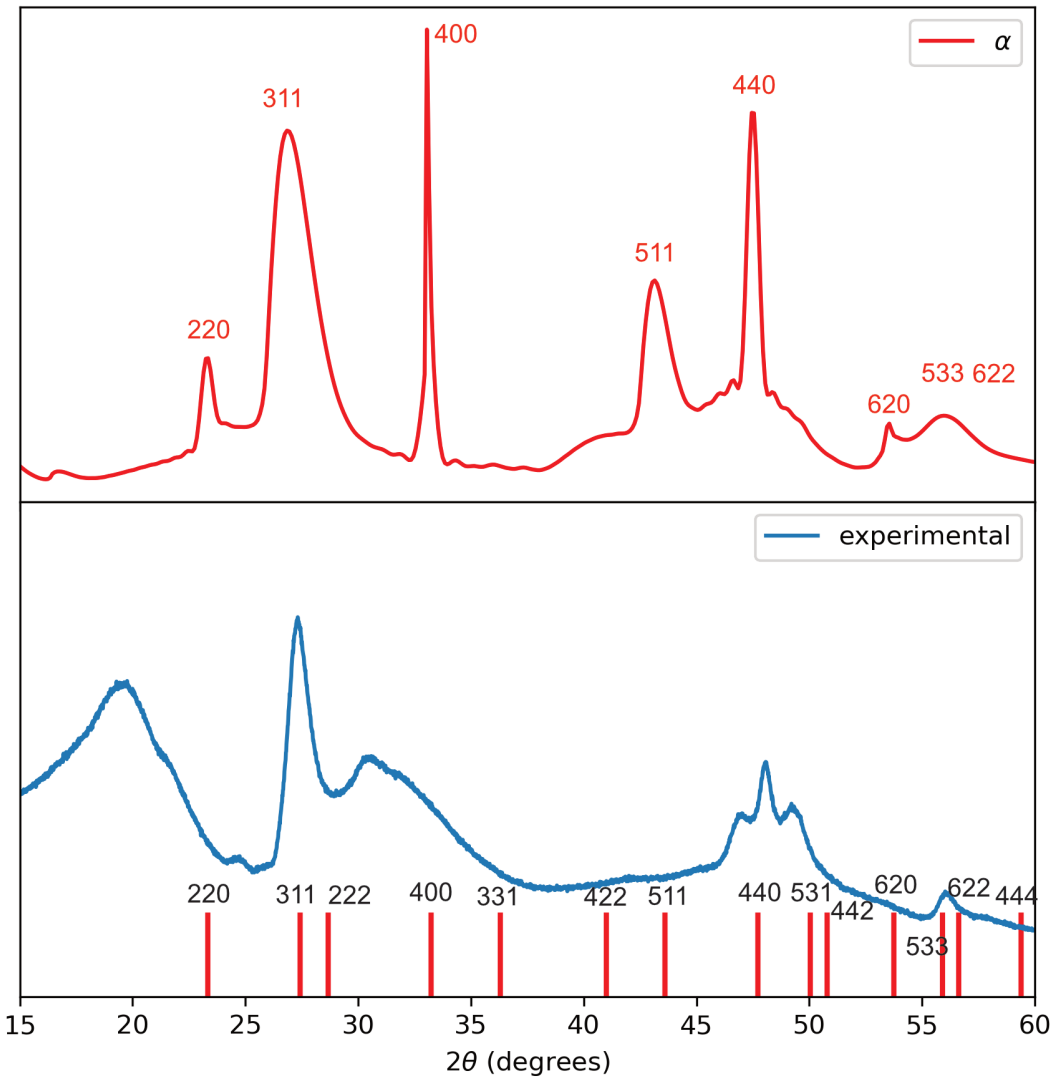

Figure S7. X-ray diffraction by the α In_2S_3 phase. The top graph shows the computed diffraction pattern (see methods in the paper for details) and the indexation of the peaks. The bottom graph shows the experimental diffraction pattern also presented in the main text along with the positions of the peaks found in file 01-084-1385 of the ICDD.

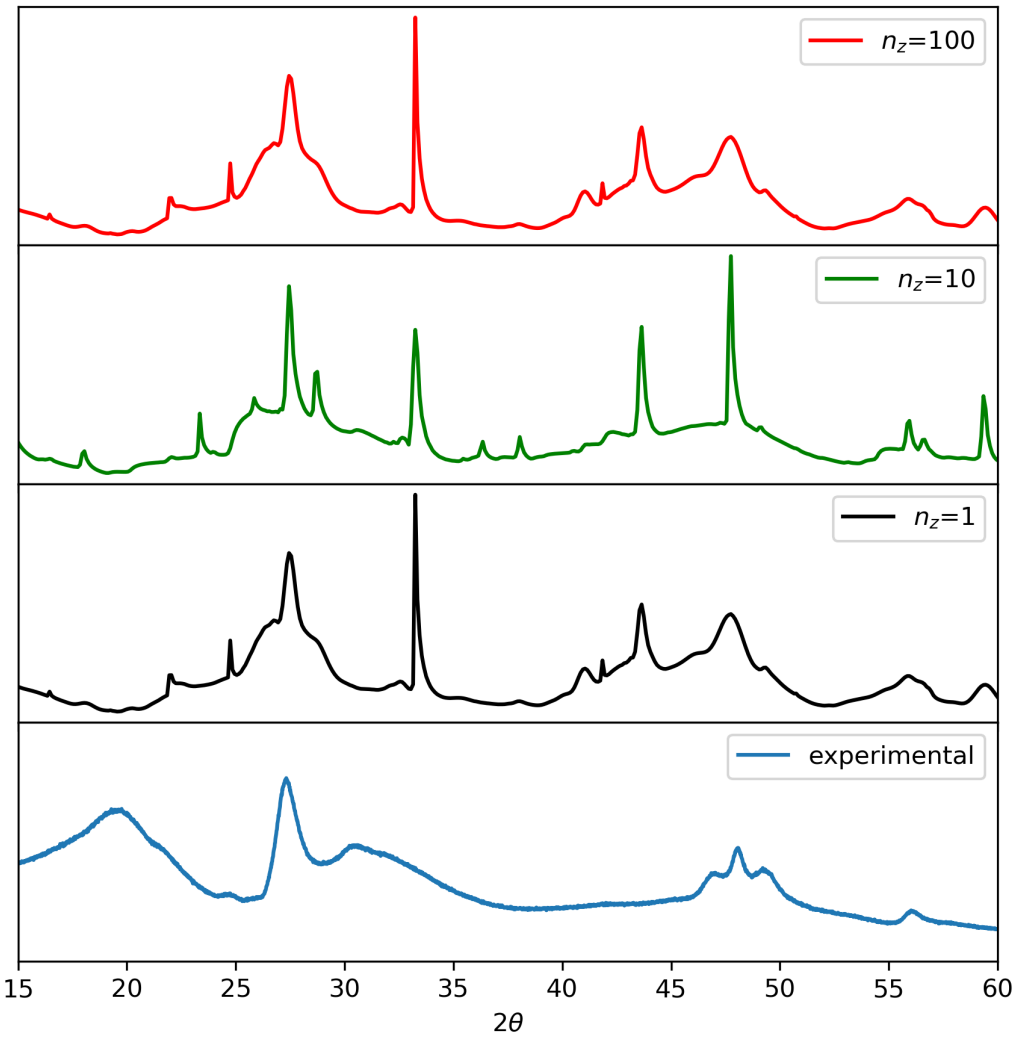

Figure S8. X-ray diffraction by the β In_2S_3 phase. The three top graphs correspond to computed diffraction patterns for different orientations of the nanoplatelets. The bottom graph shows the experimental diffraction pattern also presented in the main text.

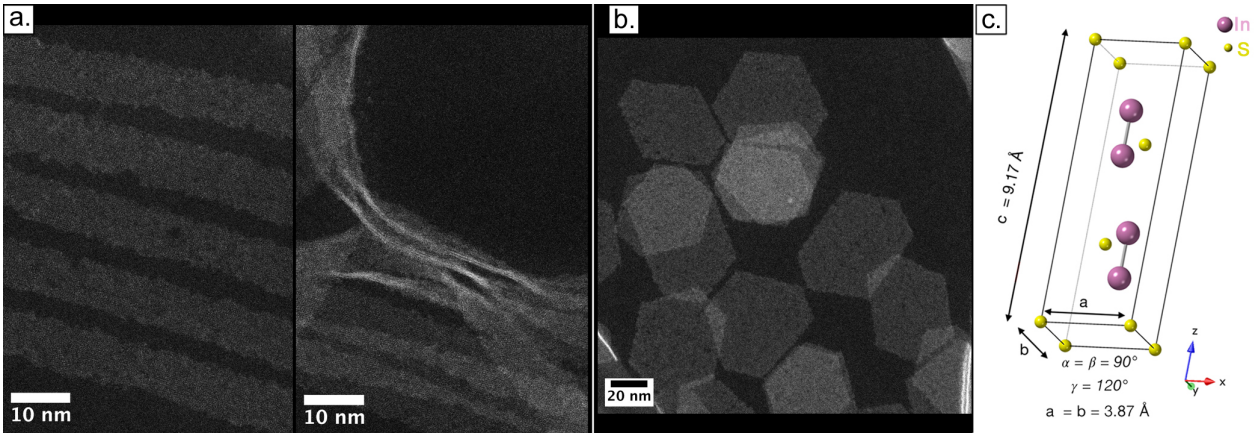

Figure S9. HAADF-STEM images of In_2S_3 (a) NR and (b) hexagons. (c) Trigonal ($P\bar{3}m1$) γ-In_2S_3 conventional-cell crystallographic representation, along with bulk referenced cell parameters.

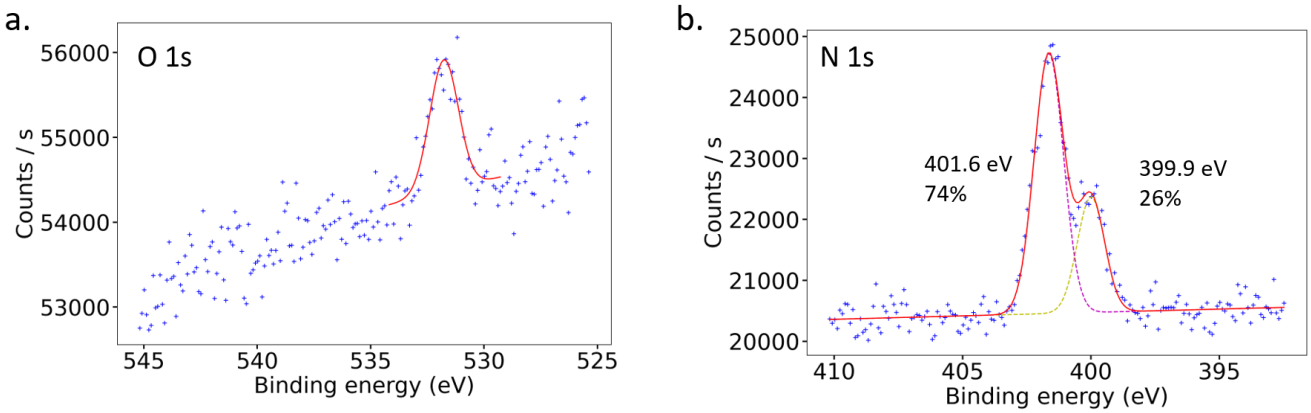

Figure S10. High-resolution XPS spectra of (a) O 1s and (d) N 1s.

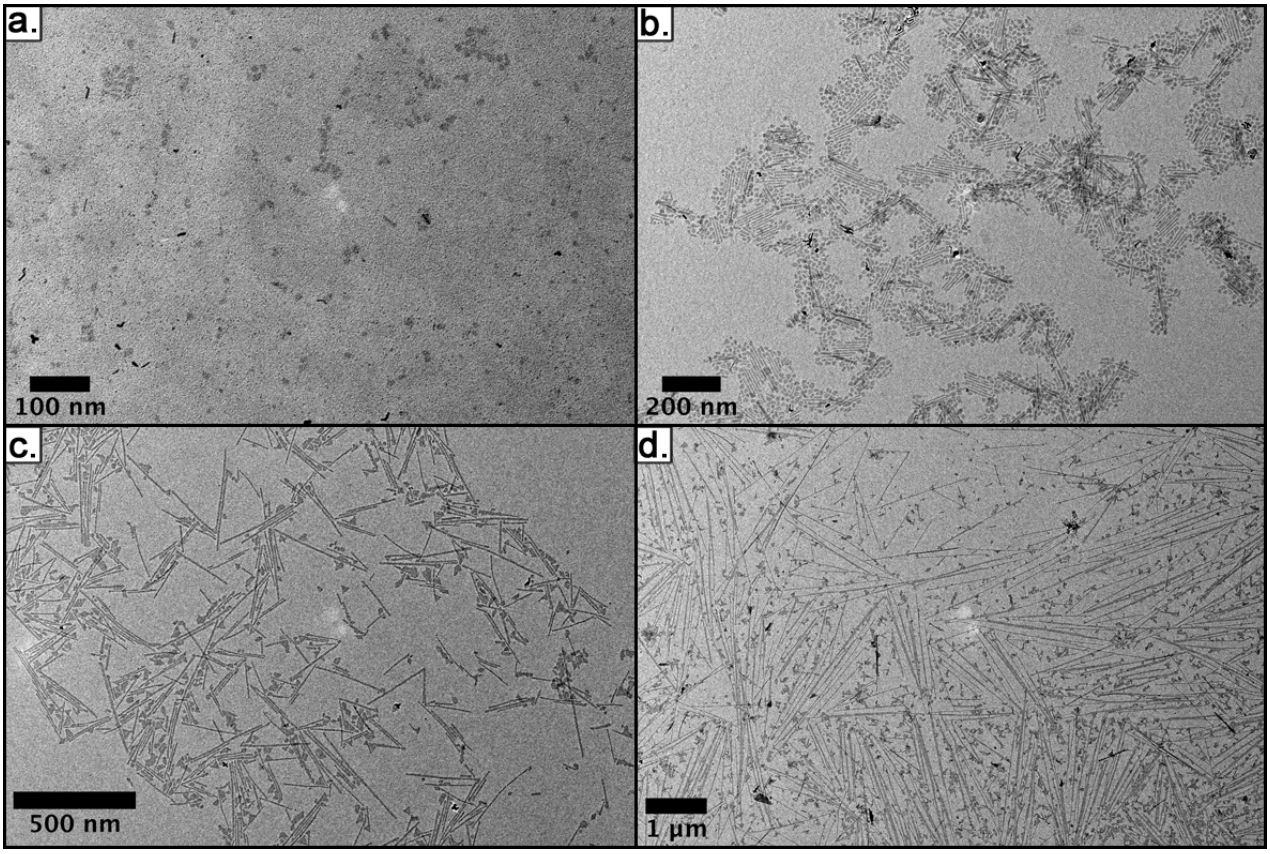

Figure S11. TEM images of the products of In_2S_3 NR reaction at different temperatures: (a) 180°C, (b) 200°C, (c) 230°C, (d) 250°C. The number and length of NR increases with the reaction temperature.

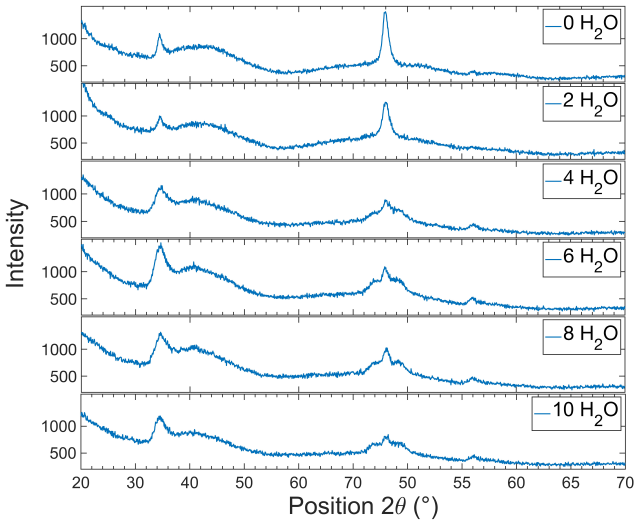

(a) Variation of the water amount

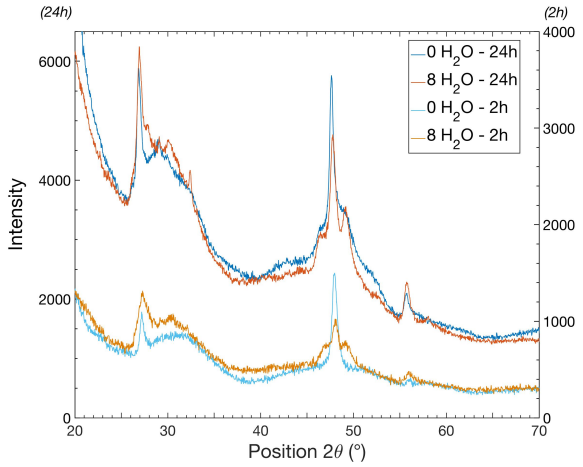

(b) Variation of the reaction time

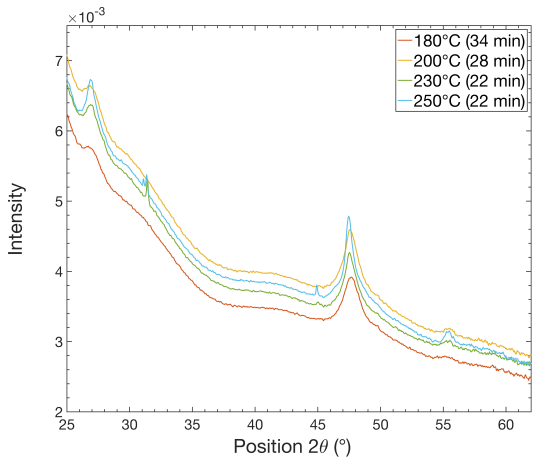

(c) Variation of the reaction temperature

Figure S12. XR diffractograms of products from the synthesis of In_2S_3 nanomaterials where:
(a.) only the amount of water is varied as regards the amount of $InCl_3$;
(b.) the reaction time is varied for respectively 0 equivalent and 8 equivalents of water used.
(c.) WAXS pattern of reaction medium at different reaction temperature and at a given reaction time.

☞ Similar XRD patterns are obtained when different amounts of water are used in the synthesis (0 to 10 equivalents as regards $InCl_3$ equivalent). Only a decrease in intensity of the peak at 48° with the amount of water added is noticed, along with the apparition of two additional peaks at 47° and 49°. These peaks might be due to different surface strains that appear as nanoribbons are obtained and get longer, increasing the anisotropy of the material. In any case, the phase is not affected by the addition of water in the reaction medium.

☞ Similar XRD patterns are also obtained for products after 2h and after 20h of reaction, for both water conditions of 0 equivalent and 8 equivalents. That shows the phase is not affected by reaction time changes and that γ-In_2S_3 is obtained in any case. Only the morphology is affected, with a change in lateral dimensions noticed on TEM images (hexagons for 0 equivalent of water and 2h of reaction – nanoribbons for all other conditions cf Fig. S16 and main text).

☞ As regard the temperature, WAXS analyses were performed for syntheses in capillaries at respectively 180 °C, 200 °C, 230 °C and 250 °C. Same diffractograms are obtained, meaning the same phase of γ-In_2S_3 is obtained, whereas a morphological change is observed on TEM images (i.e. an increase in length, width and number of NR cf Fig. S11).

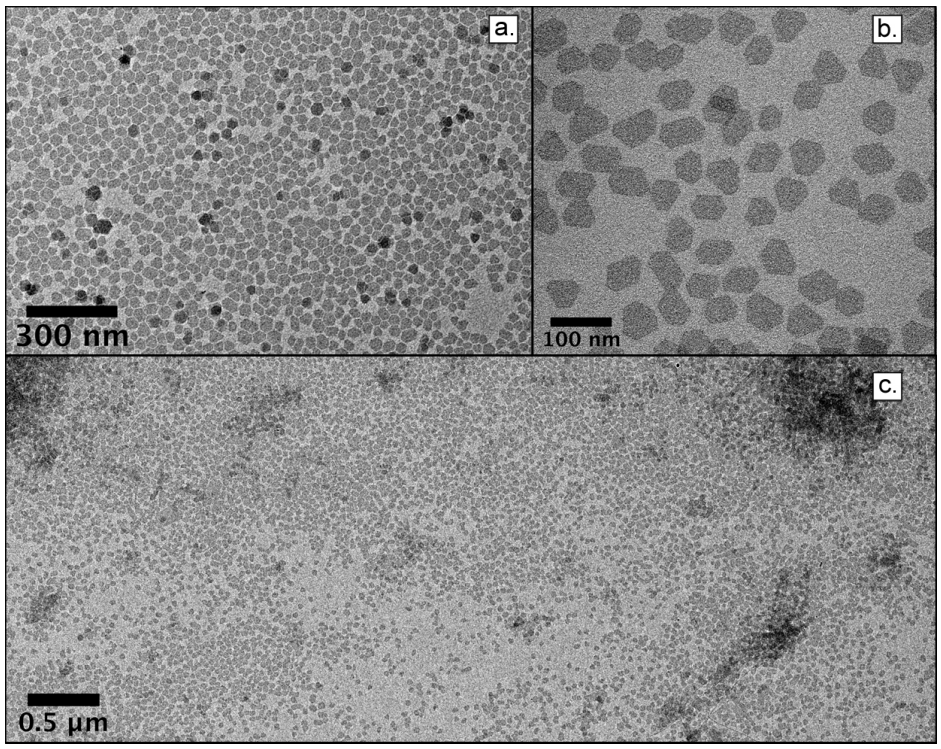

Figure S13. TEM images of In_2S_3 hexagonal NR obtained when no water is present in the initial reaction mixture.

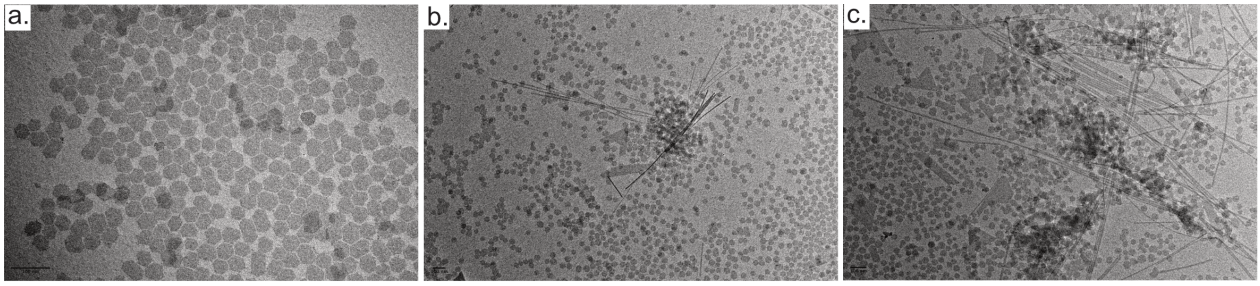

Figure S14. TEM images illustrating the effect of water addition after 2h of heating: (a) In_2S_3 hexagonal nanoplatelets after 2h of heating, (b) no water addition and 2h of further heating (4h in total), (c) addition of 8 equivalent of water with respect to indium chloride and 2h of further heating.

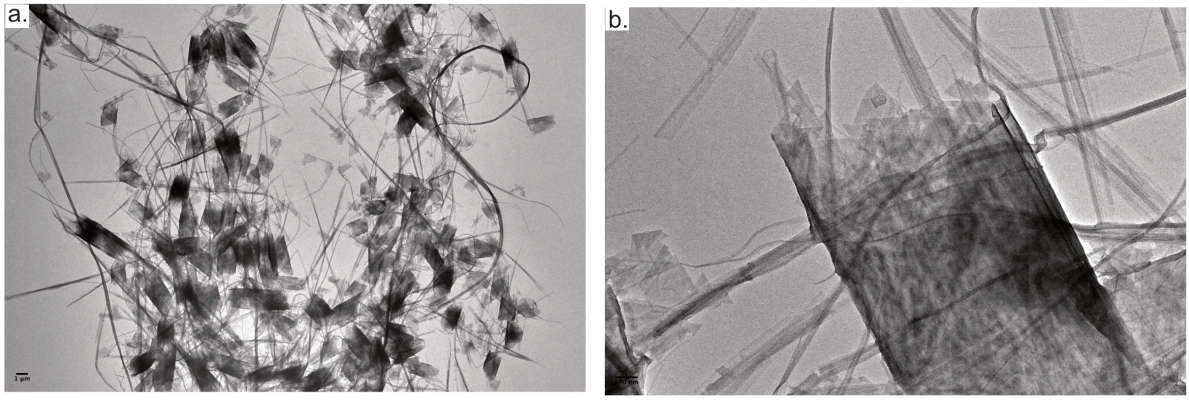

Figure S15. TEM images for In_2S_3 nanoparticles obtained after 20h under anhydrous conditions: every manipulation is performed in a glovebox except the heating.

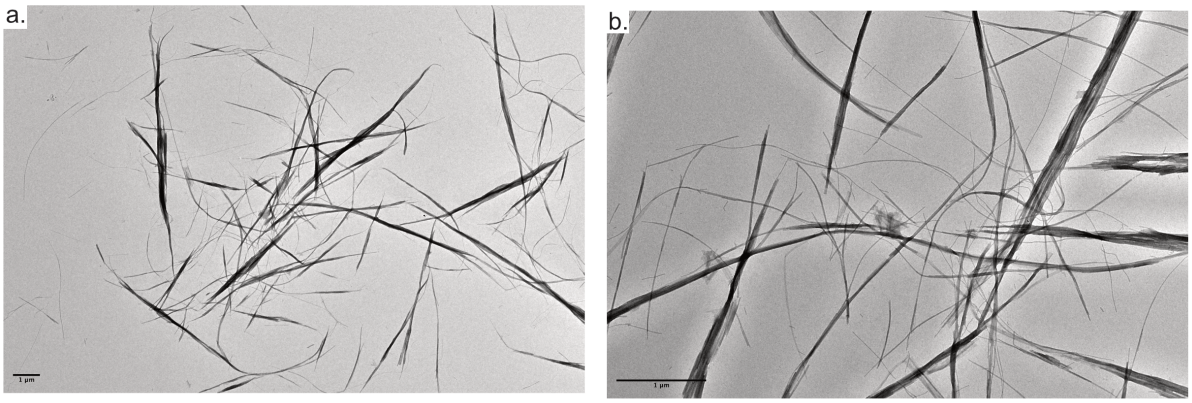

Figure S16. TEM images for In_2S_3 nanoparticles obtained after 20h under anhydrous conditions: weighing of the product and sealing of the autoclave is performed in air.

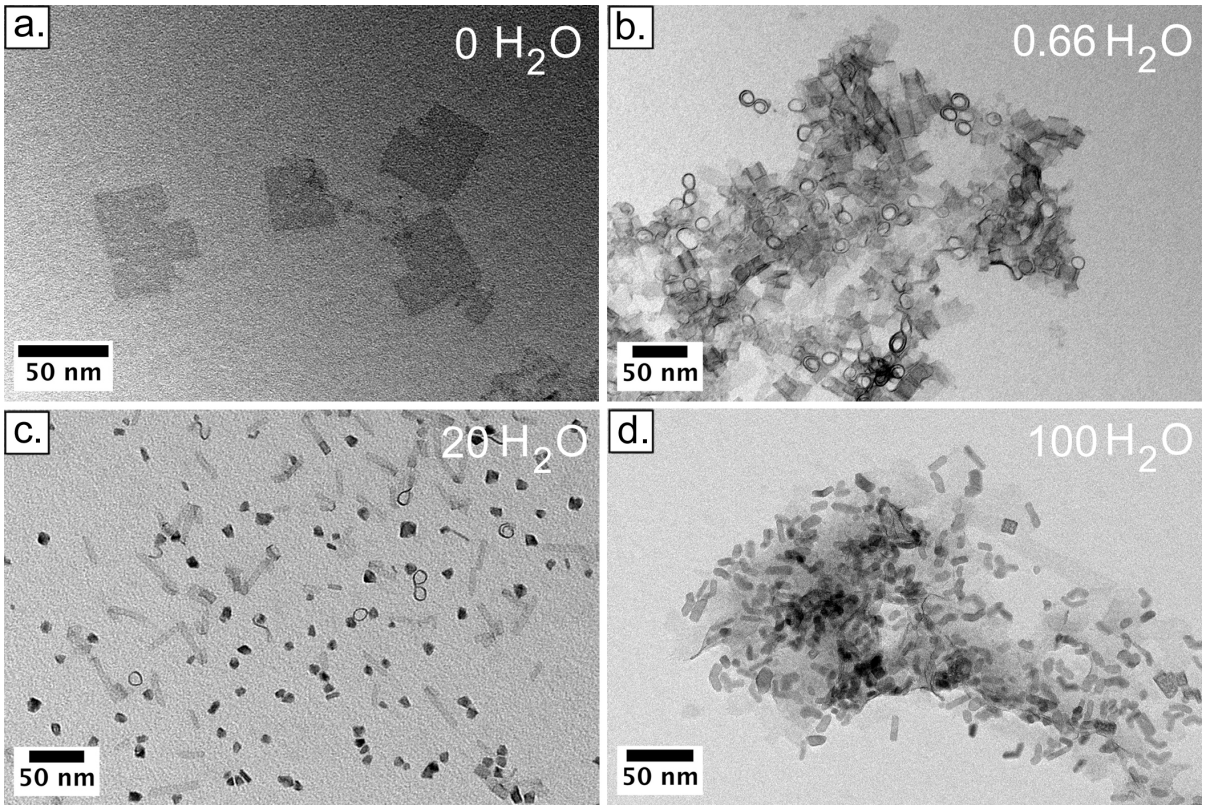

Figure S17. TEM images showing the influence of water on the morphology of indium sulfide nanoplatelets.

Figure S18. Photograph of an In_2S_3 NR dispersion at 1.3×10^{-4} volume fraction, which is right at the sol-gel transition threshold for this synthesis batch.

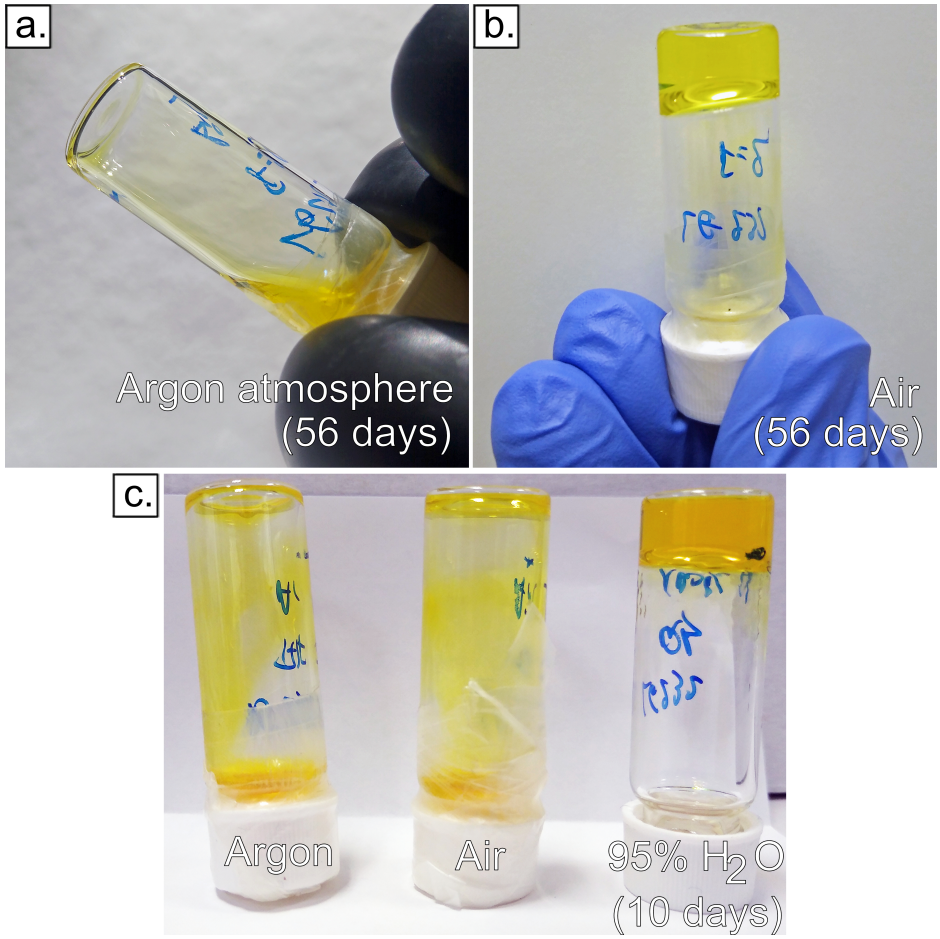

Figure S19. (a, b) In_2S_3 NR solution in THF at 10.2 g/L, after 56 days in a closed vial stored respectively (a) in glovebox under Argon atmosphere, (b) in fumehood under ambient conditions. The sample stored under ambient conditions underwent gelation, typically in 18 days. (c) In_2S_3 NR solution in THF at 20.4 g/L stored under different conditions. From left to right : under Argon, under ambient conditions or under 95% of humidity. The sample stored under Argon does not form a gel. The sample stored under air underwent gelation but several days later than the sample stored in a high humidity level atmosphere (gelation in 10 days).

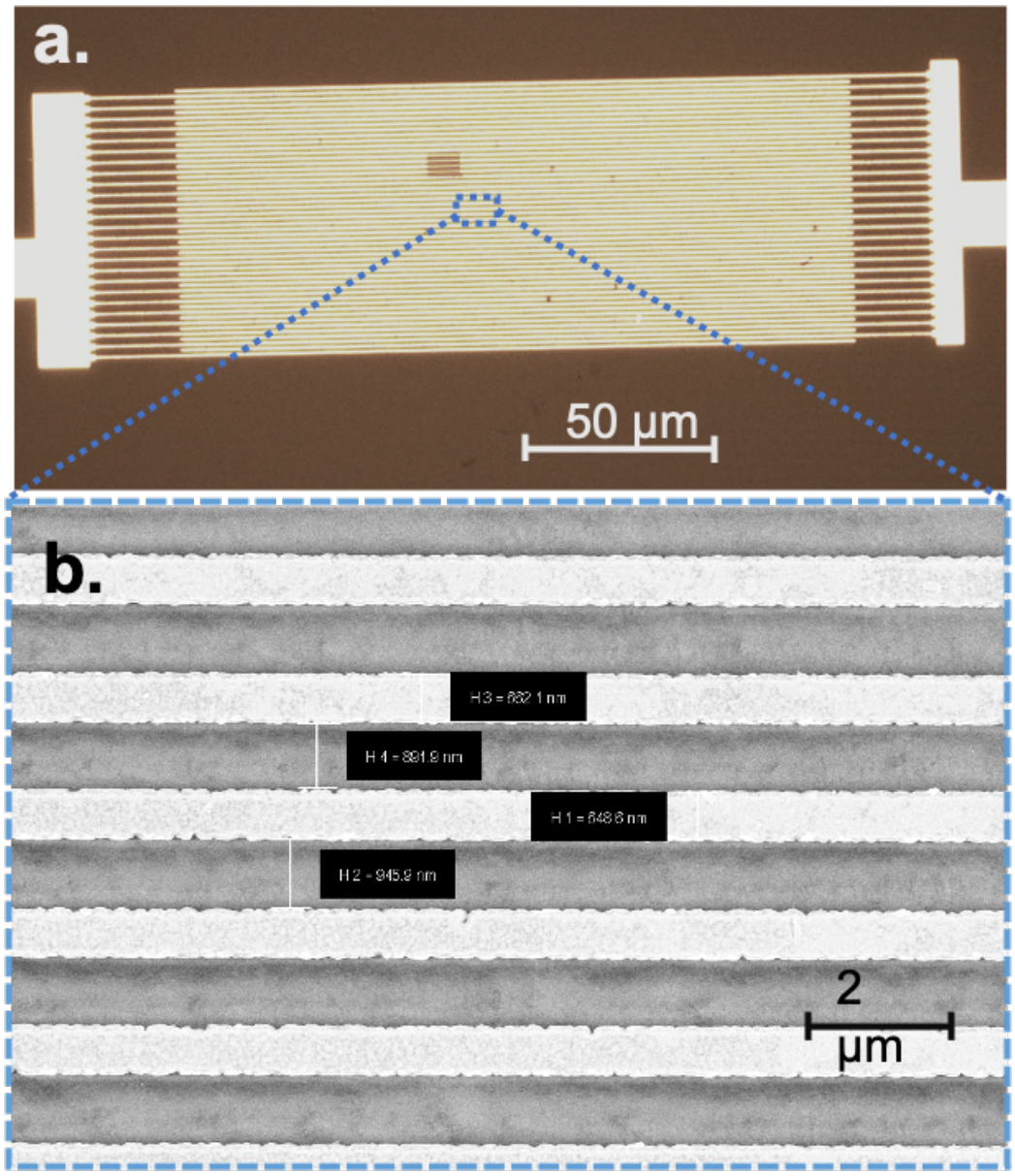

Figure S20. Interdigitated electrodes with small interelectrode spacing. (a) Optical image of the interdigitated electrodes. (b) Scanning electron microscopy image of the same electrode.